Journal of Mathematical Imaging and Vision, 4, 139–150 (1994).

Localization Properties of Direct Corner Detectors*

KARL ROHR
Arbeitsbereich Kognitive Systeme, Fachbereich Informatik, Universität Hamburg, Vogt-Kölln-Str. 30, D-22527 Hamburg, Germany

Abstract. In the past, several approaches for directly determining corners in gray-value images have been introduced. The accuracy of an approach has usually been demonstrated experimentally by comparing its results with those obtained by previous schemes. In this contribution we analyze localization properties of existing direct corner detectors by using an analytical model of gray-value corners. For the different approaches we derive implicit equations constraining the corner points and numerically evaluate their locations. Since a gray-value corner is generally defined as the curvature extremum along the edge line, we also compute this position and take it as the reference location for a comparison of the investigated approaches.

Key words. low-level vision, differential geometry, corner detection, analytical corner model, direct localization

1 Introduction

Direct approaches for detecting corners use (local) operators directly applied to the gray values without segmenting the image in advance, e.g., by concatenating edge points. Of primary interest for the application of a certain approach is the robustness, the computational expense, and the accuracy of localization. Even small measurement errors in the image plane can lead to large discrepancies in the determination of the 3D position or the shape of an object in a depicted scene. Therefore, accurately localizing prominent image features is important. In addition, if two corners are relatively close to each other, then a more accurate approach may be more helpful in resolving this situation.

In the present paper we analyze localization properties of different gray-value corner detectors applied to L-corners of a certain class. Since the quantitative model of Rohr [25], [26] is used, our results are valid for aperture angles β in the whole range of $0° < \beta < 180°$. For each approach we derive an implicit equation characterizing the localization of corner points, numerically compute the positions in the range of $0° < \beta < 180°$, and compare them with the desired position. In contrast to this, Deriche and Giraudon [9] compute the corner positions for only certain values of β and considered only some of the approaches analyzed in the present paper.

It will be shown that for the gray-value surfaces employed, the approaches considered lead to different results and that without additional steps they do not correctly localize the searched position. For general (generic) surfaces it has already been proved by Rieger [23] that the corner detector of Kitchen and Rosenfeld [16] does not find the searched position and that the corner conditions of Nagel [20] cannot be satisfied for any point.

In the following, we first discuss the usual definition of corner points. Then we describe our analytical model of an L-corner and evaluate the position of the curvature extremum along the edge line. This position will serve as a reference location for the direct approaches of Beaudet [1], Dreschler and Nagel [11], Kitchen and Rosenfeld [16], Zuniga and Haralick [30], Nagel [20], Förstner [13], Harris [22], Rohr [24], Blom et al. [5], and Brunnström et al. [7].

*This work was supported by the Deutsche Forschungsgemeinschaft (DFG) and by the European Union (EU), ESPRIT-Project VIVA (Viewpoint Invariant Visual Acquisition).

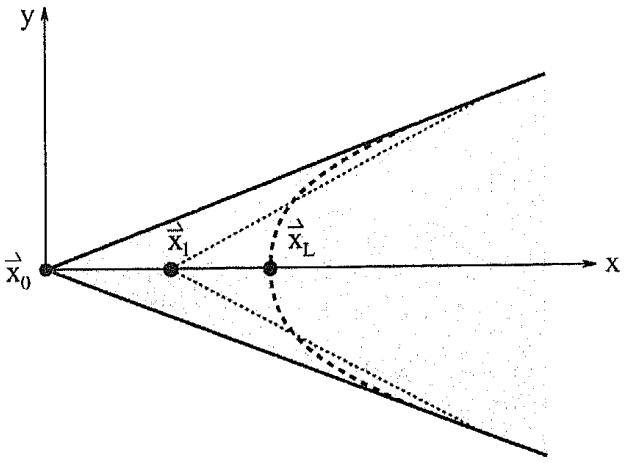

Fig. 1. Qualitative results of different approaches for finding L-corners.

2 Definition of Corner Points

Under the assumption that the 3D edges of polyhedral objects in a depicted scene are ideally sharp and that the recording camera does not disturb the intensities, a 3D corner is imaged to the solid straight lines of an L-corner in figure 1 if only two 3D edges of it are visible. The searched corner point is located at the position $\vec{x}_0$. If we take into account the blur caused by a band-limiting camera and determine those points where the gray-value gradient gets extremal in the direction of the gradient (e.g., using the approach of Canny [8] or of Korn [17]), then we qualitatively obtain the dashed curve. Now it is plausible to define the corner point $\vec{x}_L$ as the curvature extremum along this line. Indirect approaches that determine the curvature extremum along concatenated edge points as well as direct approaches in general try to determine this position. If, instead, we intersect straight lines fit to edge points, then we qualitatively obtain the point $\vec{x}_1$. Since in general the detected edge points lie inside the sector of the L-corner, $\vec{x}_1$ lies to the right of $\vec{x}_0$ and the straight line approximation yields a position of $\vec{x}_1$ to the left of $\vec{x}_L$.

The preceding argument shows that if we can assume ideal sharp edges in the scene, we should use the image position $\vec{x}_0$ for a 3D interpretation. Approaches for determining this point were introduced by Rohr [25], [26] and by Deriche and Giraudon [9]. Rohr fitted a parametric model to the observed intensities (see also [27], [28] for more efficient approaches), whereas Deriche and Giraudon exploited the results of a direct corner detector for images of different amounts of smoothing and, in addition, used the position of edge points found with the Laplacian-of-Gaussian (LoG). The classical direct corner detectors, however, try to determine the position $\vec{x}_L$ (in some cases this is assumed implicitly). Obviously, the systematic error obtained should be compensated in further interpretation steps. Since direct corner detectors are generally designed to localize the point $\vec{x}_L$, we will compare their effectiveness with respect to this position.

3 Analytical Description of an L-Corner

The mathematical description of gray-value corners in this paper supposes ideal sharp (step) transitions smoothed by a Gaussian filter. This implies, for example, ideal sharp 3D edges and the blur of the imaging system to be describable by Gaussian smoothing. A quantitative model of this kind for L-corners was introduced by Berzins [4] and is used in the work of Deriche and Giraudon [9]. A similar model can be found in [2] and [15]. These models agree with the qualitative model sketched in [10] and [20]. De Micheli et al. [19] model a Y-corner. The quantitative model of Rohr [25], [26] describes gray-value variations of an arbitrary number of intersecting edges, i.e., L-, T-, Y-, and Arrow-corners and more complex gray-value structures created by superimposing model functions of an L-corner. By fitting this model to real intensities it has been demonstrated that under certain assumptions the structural gray-value variations can adequately be described (see also [3]). Giraudon and Deriche [14] use an extension of the model in [4] and [19] for describing structures with three intersecting edges.

The model function of an L-corner in [25] and [26] exploits the symmetry of the structure with respect to the x axis (see figure 2) and is valid

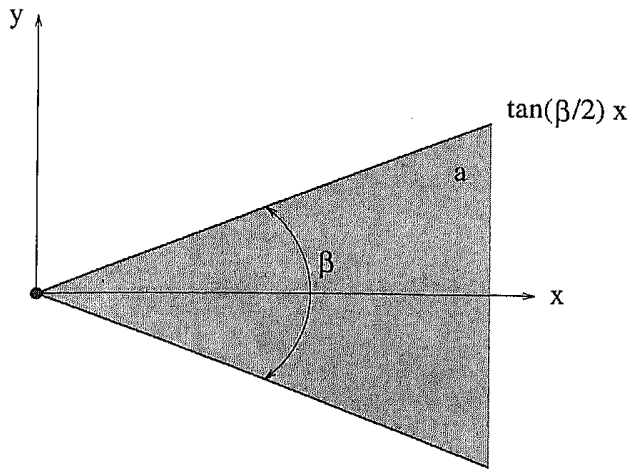

Fig. 2. Characterization of an L-corner.

for aperture angles β in the whole range of $0° < \beta < 180°$. In contrast to this, Berzins [4] derives three functions for an L-corner, the first valid for $0° < \beta < 90°$, the second valid for $\beta = 90°$, and the third valid for $90° < \beta < 180°$. Our model comprises these three functions and results from the superposition of the first function of Berzins [4] and a function obtained by reflecting this first function about the x axis. One advantage of our formulation is that the derivation of the partial derivatives of the model function we need is less tedious. Moreover, more complex corners (e.g., T-, Y-, Arrow-corners) are also obtained by superposition of model functions of the L-corner. With the image coordinates $\vec{x} = (x, y)$ and $\vec{x}^{\#} = (x, -y)$, the height of the gray-value wedge a, and the degree of smoothing $\sigma = 1$, our model of an L-corner can be described as

$$\begin{aligned} g_{\mathrm{ML}}(\vec{x}, \beta, a) &= a\big(M(\vec{x}, \beta) + M(\vec{x}^{\#}, \beta)\big) \\ &= a\big(\phi(x) - m(\vec{x}, \beta) - m(\vec{x}^{\#}, \beta)\big), \\ &\qquad 0° < \beta < 180°, \end{aligned} \tag{1}$$

where

$$\begin{aligned} M(\vec{x}, \beta) &= \phi(\vec{x}) - m(\vec{x}, \beta), \\ m(\vec{x}, \beta) &= \int_{-\infty}^{x} D(\xi, t\xi - \zeta_2)d\xi. \end{aligned}$$

Here $\phi(\vec{x}) = \phi(x)\phi(y)$, $D(\vec{x}) = G(x)\phi(y)$, $G(x)$ is the Gaussian function, $\phi(x)$ is the Gaussian error function i.e.,

$$\begin{aligned} G(x) &= \frac{1}{\sqrt{2\pi}} e^{-x^2/2}, \\ \phi(x) &= \int_{-\infty}^{x} G(\xi)d\xi, \end{aligned}$$

$t = \tan(\beta/2)$, and $\zeta_2 = tx - y$. A 3D plot of this L-corner for $\beta = 90°$, $a = 1$, and $\sigma = 1$ is depicted in figure 3.

For our comparison of corner detectors we need partial derivatives of (1). Since our model is symmetric to the x axis, the corner points are located on the line $y = 0$. Therefore in the following we only need to evaluate the x coordinates of the positions. If $q = \sqrt{1 + t^2}$, $x' = x/q$, $G_0 = G(x)/\sqrt{2\pi}$, $D_0 = G(tx')\phi(x')$, $A_0 = tx'D_0$, and $B_0 = (1 - (tx')^2)D_0$ are used, the partial derivatives of the model function for $y = 0$ calculate to

$$\begin{aligned} g_x &= \frac{2at}{q} D_0, \\ g_y &= 0, \end{aligned} \tag{2a}$$

$$\begin{aligned} g_{xx} &= \frac{2at}{q^2}(G_0 - tA_0), \\ g_{xy} &= 0, \\ g_{yy} &= -\frac{2at}{q^2}\left(G_0 + \frac{1}{t}A_0\right), \end{aligned} \tag{2b}$$

$$\begin{aligned} g_{xxx} &= -\frac{2at}{q^3}((1 + 2t^2)x'G_0 + t^2B_0), \\ g_{xxy} &= 0, \\ g_{xyy} &= \frac{2at}{q^3}(t^2x'G_0 - B_0), \\ g_{yyy} &= 0, \end{aligned} \tag{2c}$$

where the subscripts denote partial derivatives in x and y directions. To make the paper more readable we often drop the dependencies on the image coordinates $\vec{x}$.

4 Curvature Extremum Along the Edge Line

As mentioned in section 2, it is plausible to identify the corner point $\vec{x}_{\mathrm{L}}$ with the curvature extremum along the edge line (see figure 1). In our case the edge line is defined as the line

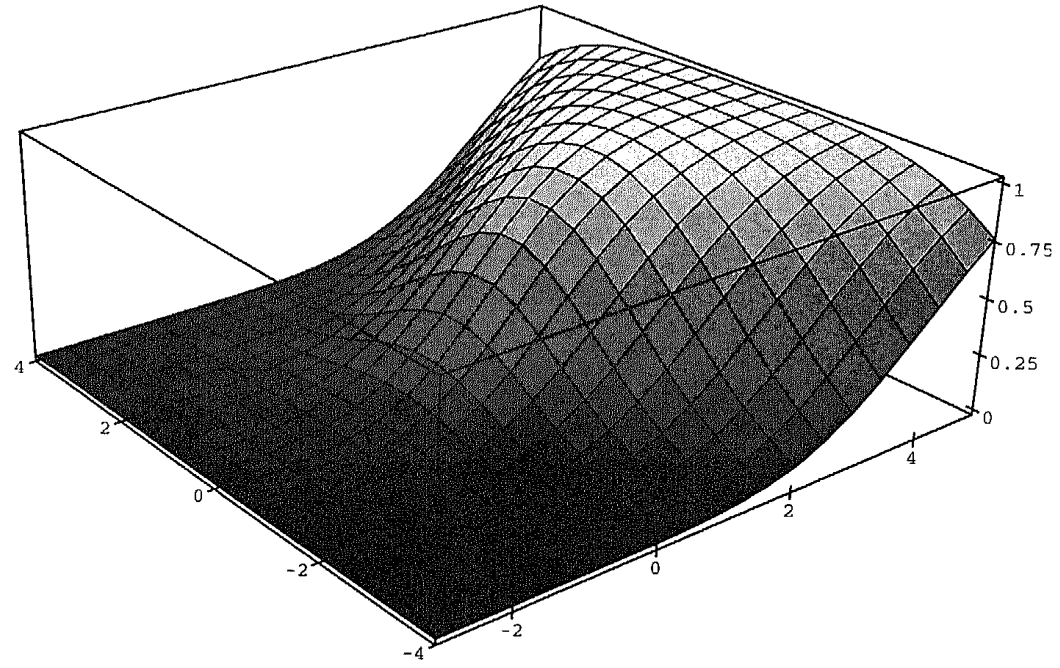

Fig. 3. 3D plot of the L-corner model ($\beta = 90°$, $a = 1$, $\sigma = 1$).

where the magnitude of the gray-value gradient becomes extremal in the direction of the gradient (sketched as the dashed curve in figure 1). With the gradient ∇g and the Hessian $\underline{H}$ expressed as

$$\nabla g = \begin{pmatrix} g_x \\ g_y \end{pmatrix},$$

$$\underline{H} = \begin{pmatrix} g_{xx} & g_{xy} \\ g_{xy} & g_{yy} \end{pmatrix},$$

the edge line is given by (see e.g., [8])

$$\begin{aligned} \Gamma(\vec{x}) &= (\nabla g)^T \underline{H} \nabla g \\ &= g_x^2 g_{xx} + 2 g_x g_y g_{xy} + g_y^2 g_{yy} = 0. \end{aligned} \quad (3)$$

The position $\vec{x}_L = (x_L, 0)$ is obtained if we intersect this line with the straight line $y = 0$. Inserting the explicitly derived partial derivatives of our model in (2) into (3), we obtain the implicit equation

$$G(x') - t^2 x' \phi(x') = 0, \quad (4)$$

which constrains x_L (see [27]). From (4) it follows that the corner position is independent of the height a. By the definition of our model this equation is valid in the whole range of $0° < \beta < 180°$. The numerically computed positions x_L as a function of β are displayed in figure 12 in section 6 (bold-faced curve; x_0 assumed to be located at $x = 0$). If $\beta = 90°$, for example, we get $x_L = 0.71567$. Positions for different amounts of smoothing σ are obtained by scaling the x coordinates; e.g., doubling the value of σ leads to twice the value of x_L.

Although it is intuitively plausible, we are not sure that $\vec{x}_L$ actually is a curvature extremum. For general (generic) surfaces Rieger [23] has shown that the necessary condition for a curvature extremum along $\Gamma(\vec{x}) = 0$ consists of several hundred terms containing partial derivatives up to the fifth order. Here, we derive this condition by using implicit differentiation and show for our L-corner model that this condition is actually satisfied in $\vec{x}_L$.

If, in a certain point on an implicitly given curve $\Gamma(\vec{x}) = 0$, we have $\Gamma_x(\vec{x}) \neq 0$, then in a small neighborhood of this point there exists a

function $x = x(y)$ such that $\Gamma(x(y), y) = 0$ and

$$x_y(y) = -\frac{\Gamma_y(x(y), y)}{\Gamma_x(x(y), y)} \tag{5}$$

[6]. In our case we have $\Gamma_x(\vec{x}_L) = g_x^2 g_{xxx} < 0$ since $g_x = ((2at)/q)G(tx')\phi(x') > 0$ and $g_{xxx} = -((2at^3)/q^3)(1 + x^2)G(tx')\phi(x') < 0$ in $\vec{x}_L$ (for $t > 0$ and $a > 0$), and therefore (5) is valid. Repeated differentiation of (5) leads to $x_{yy}(y)$ and $x_{yyy}(y)$. For a curvature extremum along $x(y)$ the derivative of the curvature $\kappa(y)$ must vanish:

$$\begin{aligned}\kappa_y(y) &= \frac{d}{dy}\left(\frac{x_{yy}(y)}{(1 + x_y^2(y))^{3/2}}\right) \\ &= \frac{(1 + x_y^2(y))x_{yyy}(y) - 3x_y(y)x_{yy}^2(y)}{(1 + x_y^2(y))^{5/2}} \\ &= 0,\end{aligned} \tag{6}$$

i.e.,

$$(1 + x_y^2(y))x_{yyy}(y) - 3x_y(y)x_{yy}^2(y) = 0. \tag{7}$$

To show that this condition is satisfied in $\vec{x}_L$ for our L-corner model, we exploit the symmetry of the model function with respect to the x axis (cf. (1)) and apply a lemma of Whitney. This lemma states that for a locally differentiable C^∞ function $f(x, y)$ that is even in y (i.e., $f(x, -y) = f(x, y)$) there exists a function $\tilde{f}(x, y)$ such that $f(x, y) = \tilde{f}(x, y^2)$ [18]. No method is given for constructing $\tilde{f}(x, y)$. However, by using Whitney's Lemma we can get information about the partial derivatives of $f(x, y)$ without knowing $\tilde{f}(x, y)$ (and without the need for evaluating the partial derivatives of $f(x, y)$ explicitly).

For our model we obtain the partial derivatives as listed in the appendix. Setting $y = 0$, we get $g_y = g_{xy} = g_{xxy} = g_{yyy} = 0$, which is in accordance with (2). If, in addition, we use the knowledge that g_x is extremal in $\vec{x}_L$, i.e. that $g_{xx} = 0$ ($\vec{x}_L$ must lie on $\Gamma(\vec{x})$ and therefore (3) has to be satisfied), then the very extensive general condition for a curvature extremum reduces to

$$\begin{aligned}&3g_{xxxy}(g_x^2 g_{xxyy} + 2g_{yy}(2g_x g_{xyy} + g_{yy}^2)) \\ &\quad - g_x g_{xxx}(6g_{yy}g_{xyyy} + g_x g_{xxyyy} = 0.\end{aligned} \tag{8}$$

If we also use the information of vanishing fourth-order derivatives for $y = 0$ ($g_{xxxy} = g_{xyyy} = 0$), we get

$$g_x^2 g_{xxx} g_{xxyyy} = 0, \tag{9}$$

which is actually valid since $g_{xxyyy} = 0$. Thus the condition for a curvature extremum in $\vec{x}_L$ is satisfied. Assuming that terms of the sum do not compensate, we see that partial derivatives of the fifth order are really necessary to determine $\vec{x}_L$.

5 Direct Approaches for Determining Corners

5.1 Beaudet (1978)

The approach of Beaudet [1] exploits the determinant of the Hessian matrix $\underline{H}$, which gives significant values near corners. Therefore we have to determine local extrema

$$\begin{aligned}\mathrm{DET}(\vec{x}) &= \det \underline{H} \\ &= g_{xx}g_{yy} - g_{xy}^2 \rightarrow \text{extremum},\end{aligned} \tag{10}$$

which satisfy the necessary conditions $\mathrm{DET}_x = \mathrm{DET}_y = 0$. For our analytical L-corner model and for $y = 0$ these conditions lead to

$$g_{xx}g_{xyy} + g_{yy}g_{xxx} = 0. \tag{11}$$

From the preceding equation we get the implicit equation

$$\begin{aligned}&(1 + 3t^2)x'G^2(x') \\ &\quad + \left((-1 + t^2) + (1 + 3t^2 - 2t^4)x'^2\right) \\ &\quad \times G(x')\phi(x') \\ &\quad + 2t^2x'(1 - (tx')^2)\phi^2(x') = 0,\end{aligned} \tag{12}$$

which has two solutions, a negative local extremum and a positive local extremum (x_{Bn} and x_{Bp}; hyperbolic and elliptic points of the gray-value surface). For different aperture angles β and smoothing values σ these extrema are displaced. Setting $\beta = 90°$ ($t = 1$, $q = \sqrt{2}$) with $x^* = x/\sqrt{2}$, we obtain the equation

$$\begin{aligned}&x^*\left(2G^2(x^*) + x^*G(x^*)\phi(x^*)\right. \\ &\quad \left. + (1 - x^{*2})\phi^2(x^*)\right) = 0,\end{aligned} \tag{13}$$

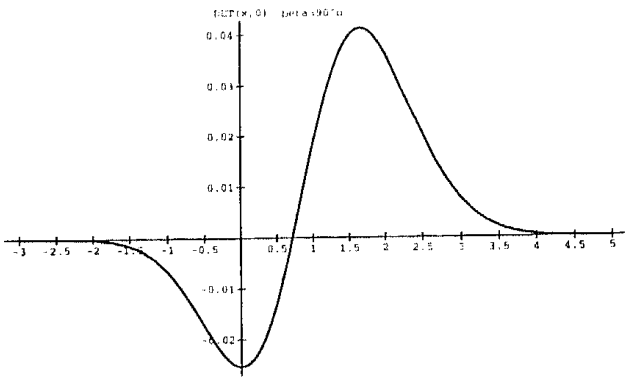

Fig. 4. DET(x, 0) for $\beta = 90°$.

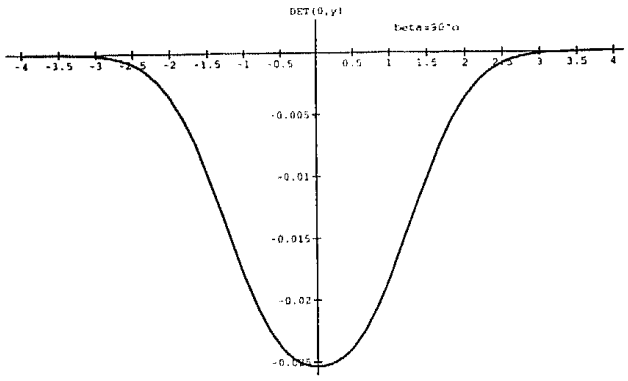

Fig. 5. DET(0, y) for $\beta = 90°$.

for which the first solution, $x_{Bn} = 0$, is obvious. The second solution, $x_{Bp} = 1.65653$, has been determined numerically. The graph of DET for $\beta = 90°$ and $y = 0$ is displayed in figure 4. The positions x_{Bn} and x_{Bp} as a function of β are plotted in figure 12 in section 6 (lightface solid curves).

It should be noted that Deriche and Giraudon [9] claim that x_{Bn} is not a local extremum in all directions. This is intuitively hard to understand, especially if we look at the graph of DET for $\beta = 90°$ at $x_{Bn} = 0$ in the y direction (figure 5), which exhibits a local extremum in this direction also. For the special case of $\beta = 90°$ the Hessian of DET in x_{Bn} is $\mathrm{DET}_{xx}\mathrm{DET}_{yy} - \mathrm{DET}_{xy}^2 = (16 - \pi^2)/(8\pi^2)^2 > 0$. Since $\mathrm{DET}_{xx} = (4 + \pi)/(8\pi^2) > 0$, DET surely has a local minimum in x_{Bn} (a 2D function $f(\vec{x})$ has a local minimum if $f_{xx}f_{yy} - f_{xy}^2 > 0$ and $f_{xx} > 0$ holds at a certain point). A proof for general values of β leads to very lengthy calculations that we have not yet been able to carry out.

5.2 *Dreschler and Nagel (1981)*

Dreschler and Nagel [11] describe an approach that exploits the local extrema of DET (see also [20] and [29]). At x_L (the point of extremal curvature in the line with maximal gradient in the direction of the gradient) we have DET = 0 since at this point we have $g_{xx} = g_{xy} = 0$. Dreschler and Nagel [11] interpolate the local extrema of DET in order to find the position x_L (see [10]). If the interpolation could be performed exactly, then, indeed, the position $x_{DN} = x_L$ would be obtained. Using linear interpolation (which is more realistic in comparison with the actual implementation), for $\beta = 90°$ we obtain the position $x_{DN} = (x_{Bn} + x_{Bp})/2 \approx 0.82826$. The positions for general values of β, also computed by using linear interpolation, are depicted in figure 12 in section 6.

5.3 *Kitchen and Rosenfeld (1982)*

With the gradient magnitude $|\nabla g| = \sqrt{\nabla g^2}$ and the vector $\nabla g^\perp = (-g_y, g_x)^T$ perpendicular to the gradient, the differential operator of Kitchen and Rosenfeld [16] consists of

$$\begin{aligned} \mathrm{KR}(\vec{x}) &= \frac{(\nabla g^\perp)^T \underline{H} \nabla g^\perp}{|\nabla g|^2} \\ &= \frac{g_x^2 g_{yy} - 2g_x g_y g_{xy} + g_y^2 g_{xx}}{g_x^2 + g_y^2} \\ &\rightarrow \text{extremum} \end{aligned} \tag{14}$$

and represents the curvature of a plane curve (isophote, level curve) multiplied by $|\nabla g|$. For $y = 0$ the conditions $\mathrm{KR}_x = \mathrm{KR}_y = 0$ result in $g_{xyy} = 0$ and therefore in

$$t^2 x' G(x') - (1 - (tx')^2)\phi(x') = 0, \tag{15}$$

which yields the corner positions x_{KR} represented by the boldfaced dashed curve in figure 12 of section 6. For $\beta = 90°$ we get $x_{KR} = 1.18783$ (see figure 6). To improve the accuracy of localization Kitchen and Rosenfeld [16] propose

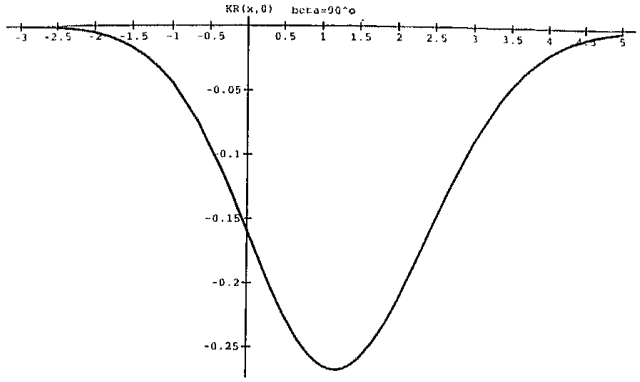

Fig. 6. KR(x, 0) for $\beta = 90°$.

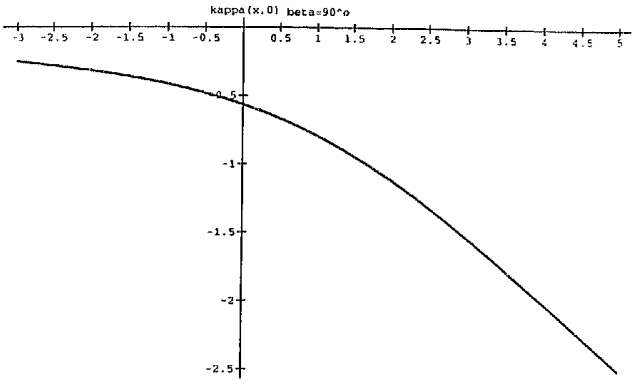

Fig. 7. $\kappa(x, 0)$ for $\beta = 90°$.

considering only edge points (maximal gradient in the direction of the gradient) as candidates for corners. With this additional step the searched corner position $x_{KR} = x_L$ actually would be obtained if the edge points could be localized exactly.

5.4 *Zuniga and Haralick (1983)*

Zuniga and Haralick [30], in contrast to Kitchen and Rosenfeld [16], directly use the curvature of a plane curve

$$\kappa(\vec{x}) = \frac{(\nabla g^{\perp})^T \underline{H} \nabla g^{\perp}}{|\nabla g|^3} = \frac{\mathrm{KR}(\vec{x})}{|\nabla g|} \rightarrow \text{extremum} \qquad (16)$$

under the assumption that only edge points are considered as candidates for corners. Somewhat surprisingly, the application of their operator does not yield an extremum in x direction on $y = 0$ (see figure 7 for $\beta = 90°$); i.e., the conditions derived from (16),

$$g_x g_{xyy} - g_{xx} g_{yy} = 0 \qquad (17)$$

and

$$G^2(x') + x' G(x') \phi(x') - \phi^2(x') = 0, \qquad (18)$$

cannot be fulfilled. Therefore, for detecting corners, the extremal property of $\kappa(\vec{x})$ is exploited only in y direction. The localization in x direction relies merely on the determination of edge positions.

5.5 *Nagel (1983)*

Nagel [20] proposes determination of corners by the following conditions:

$$\begin{aligned} g_x &\rightarrow \text{extremum}, & g_y &= 0, \\ g_{xx} &= 0, & g_{yy} &\rightarrow \text{extremum}, \end{aligned} \qquad (19)$$

where the local coordinate system should be aligned in such a way that $g_{xy} = 0$. From these conditions the following equations can be obtained:

$$g_y = 0, \qquad (20a)$$
$$g_{xx} = 0, \qquad (20b)$$
$$g_{xyy} = 0, \qquad (20c)$$
$$g_{yyy} = 0. \qquad (20d)$$

After the coordinate system has been fixed (here $g_{xy} = 0$), these four conditions have to be satisfied at corners (and, moreover, all other points should be excluded by these conditions). However, already two conditions uniquely determine a point on a sufficiently general 2D surface. Therefore for general (generic) surfaces all four conditions in (20) can never be satisfied in any point (see [23]). For special surfaces, however, it could be possible that these conditions are fulfilled.

In the following we consider the conditions of Nagel [20] for the special surfaces of our L-corner model. From (2) we see that $g_{xy} = 0$ holds for $y = 0$; i.e., the local coordinate system

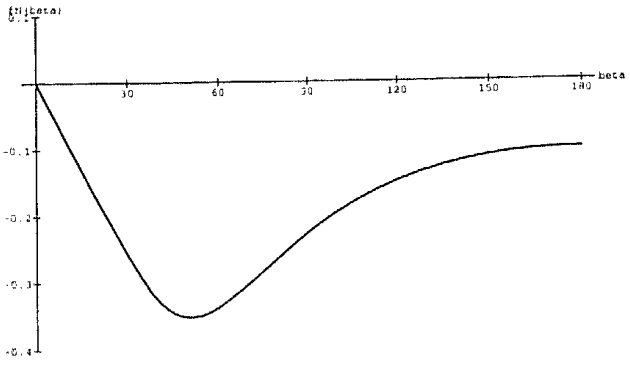

Fig. 8. $f_N(\beta)$.

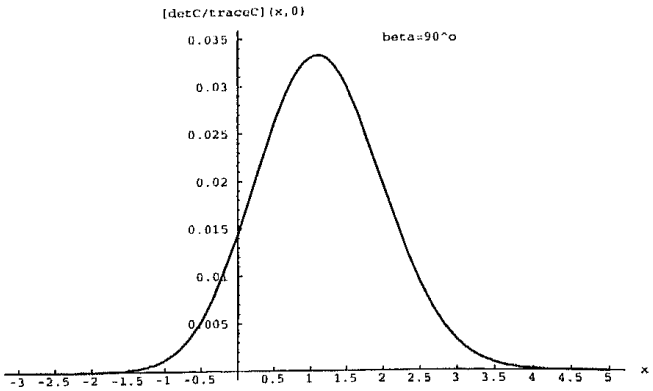

Fig. 9. $[\det \underline{C}/\mathrm{trace}\,\underline{C}]\ (x, 0)$ for $\beta = 90°$.

is fixed as required in [20]. Also, for all points on $y = 0$ we have $g_y = g_{yyy} = 0$. Therefore conditions (20a) and (20d) are satisfied. If, in addition, we require condition (20b) to be fulfilled, we get the position x_L defined by (4). At this point we have

$$g_{xyy} = \frac{2at}{q^3}((tx)^2 - 1)D_0, \tag{21}$$

and setting this partial derivative to zero (condition (20c)) yields $x_N = 1/t(t > 0)$. Choosing $\beta = 90°$ gives $x_N = 1$, which does not satisfy condition (20b) since the solution of this condition evaluates to $x_L \approx 0.71567$ (see section 4). For arbitrary values of β and simultaneously satisfying conditions (20b) and (20c),

$$f_N(\beta) = G\left(\frac{1}{tq}\right) - \frac{t}{q}\phi\left(\frac{1}{tq}\right) = 0 \tag{22}$$

has to be fulfilled. Plotting $f_N(\beta)$ reveals that (22) is fulfilled only for $\beta = 0$ (figure 8); i.e., for all L-corners there is no point on $y = 0$ that satisfies the conditions of Nagel [20].

5.6 Förstner (1986), Harris (1987), and Rohr (1987)

The corner detectors of Förstner [13] and Harris (Plessey corner detector; see Noble [22]) use the matrix

$$\underline{C} = \begin{pmatrix} \overline{g_x^2} & \overline{g_x g_y} \\ \overline{g_x g_y} & \overline{g_y^2} \end{pmatrix}, \tag{23}$$

which represents average values of components of the gray-value gradient. This matrix results from a straightforward generalization from 1D to 2D of the considerations in Förstner [12] concerning the geometric precision of correlation methods. Developing the gray-value gradient up to a first-order expansion yields the matrix

$$\underline{C} \approx \nabla g(\nabla g)^T + c\underline{H}^2 \tag{24}$$

in [21], which has been used in [24] for detecting corners. The parameter c is a measure for the size of the area over which the gradient components are averaged. For all approaches analyzed in this section we use the expression in (24), where it is understood that this is an approximation to (23).

To detect corners Förstner [13] evaluates

$$\frac{\det \underline{C}}{\mathrm{trace}\,\underline{C}}(\vec{x}) \rightarrow \text{maximum}. \tag{25}$$

This is equivalent to minimizing the inverse of (25), as done by Harris [22]. For our L-corner model, the graph of $\det \underline{C}/\mathrm{trace}\,\underline{C}(\vec{x})$ for $\beta = 90°$ on $y = 0$ is depicted in figure 9. Setting the partial derivatives of (25) equal to zero for $y = 0$ yields the requirement

$$g_x^4 g_{xyy} + c g_{xx}(g_x(2g_x g_{xx} g_{xyy} + g_{yy}^3) + c(g_{xx}^3 g_{xyy} + g_{yy}^3 g_{xxx})) = 0. \tag{26}$$

The localized positions x_F can be seen in figure 12 of section 6 (light face dashed curve). Here, we assume 3×3 operators in (24), for

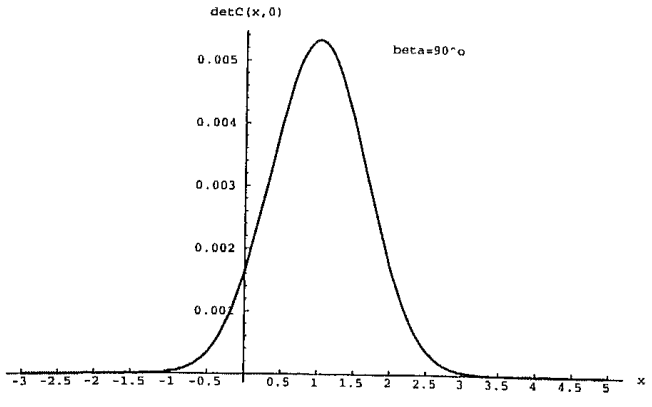

Fig. 10. $\det \underline{C}\ (x, 0)$ for $\beta = 90°$.

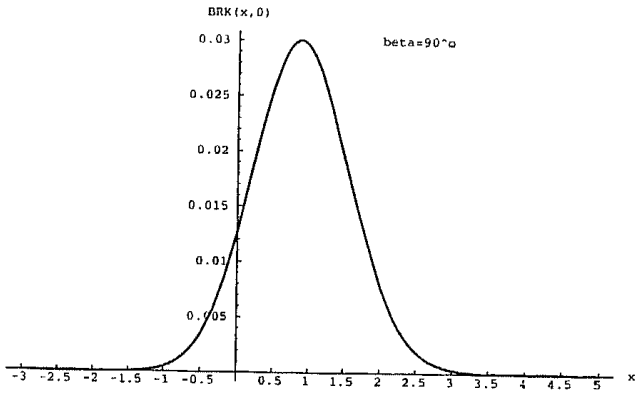

Fig. 11. BRK$(x, 0)$ for $\beta = 90°$.

which we have $c = 2/3$. For $\beta = 90°$ the position is $x_F = 1.09673$.

The corner detector of Rohr [24] (see also [26]) evaluates

$$\det \underline{C}(\vec{x}) \rightarrow \text{maximum}, \tag{27}$$

which gives the condition

$$g_x(g_x g_{xyy} + g_{xx} g_{yy}) + c g_{xx}(g_{xx} g_{xyy} + g_{yy} g_{xxx}) = 0. \tag{28}$$

The localized points x_R with this approach are also displayed in figure 12 of section 6 (lightface dotted curve). For $\beta = 90°$ we have $x_R = 1.01947$ (see also figure 10).

5.7 Blom et al. (1992) and Brunnström et al. (1992)

Recently, Blom et al. [5] introduced a new direct corner detector that is a modified version of the one proposed by Kitchen and Rosenfeld [16]. Their cornerness measure,

$$\text{BRK}(\vec{x}) = -(\nabla g^{\perp})^T \underline{H} \nabla g^{\perp} \rightarrow \text{extremum}, \tag{29}$$

is the numerator of (14) and has been chosen in such a way that the detector satisfies a certain invariance property. The same cornerness measure is also used in Brunnström et al. [7]. The graph of this measure for $\beta = 90°$ on $y = 0$ is depicted in figure 11. From (29) we obtain

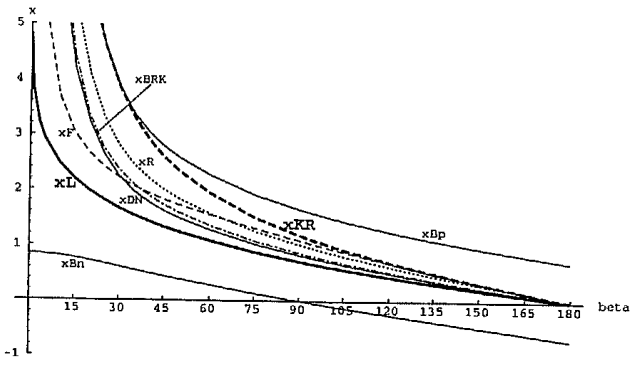

Fig. 12. Localization results of different approaches.

the conditions

$$g_x g_{xyy} + 2 g_{xx} g_{yy} = 0 \tag{30}$$

and

$$2G^2(x') + (2 - 3t^2) x' G(x') \phi(x') + (1 - 3(tx')^2) \phi^2(x') = 0 \tag{31}$$

and the corner positions x_{BRK} as plotted in Figure 12 of section 6 (lightface dashed-dotted curve). For $\beta = 90°$ the position is $x_{BRK} = 0.86849$.

6 Comparison and Discussion

Figure 12 shows the localized positions x of the different approaches as functions of the aperture angle β for our L-corner model on the symmetry line $y = 0$ and for a Gaussian blur of $\sigma =$

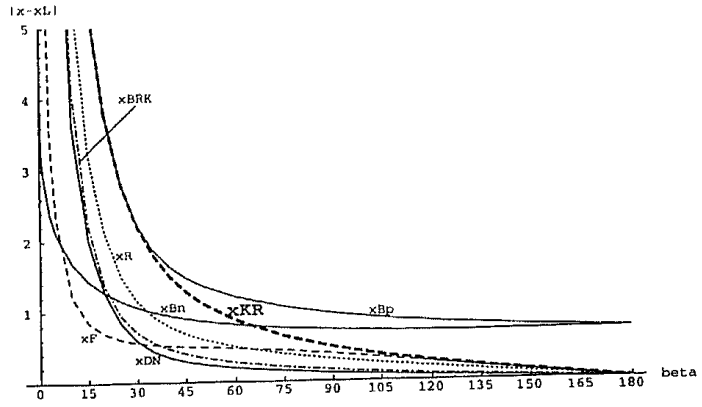

Fig. 13. Absolute deviations from x_L for the approaches in figure 12.

1. Positions for different amounts of blur are obtained by $x(\sigma) = x\sigma$. The height a of the L-corner has no influence on the positions.

From figure 12 we see that, with the exception of the negative extremum x_{Bn} of DET, when the approach of Beaudet [1] is used all localized positions are larger than x_L (as the curvature extremum along the line with maximal gradient in the direction of the gradient) and for $\beta \to 0$ they move to ∞. The absolute deviations of the positions to x_L are shown in figure 13. Dreschler and Nagel [11] determine the corner point by interpolating the two extrema of Beaudet [1]. The positions found by linear interpolation are for aperture angles $\beta \gtrsim 30°$, the closest to x_L. With an exact interpolation the desired position $x_{DN} = x_L$ would actually be obtained. On the other hand, to find x_L the position of edge points could be incorporated in the manner of Kitchen and Rosenfeld [16] or of Zuniga and Haralick [30]. However, when edge points are exploited, all other approaches investigated in this paper (with the exception of Nagel [20]) also would find x_L. The operator of Beaudet [1] could be treated analogously if we separately considered the negative or the positive extremum of DET.

If such additional steps (interpolation or incorporation of edge points) are disregarded and only measures that have to be maximized or minimized are considered (this is what we are really looking for), the following can be said. For reasons of clarity, we have selected the

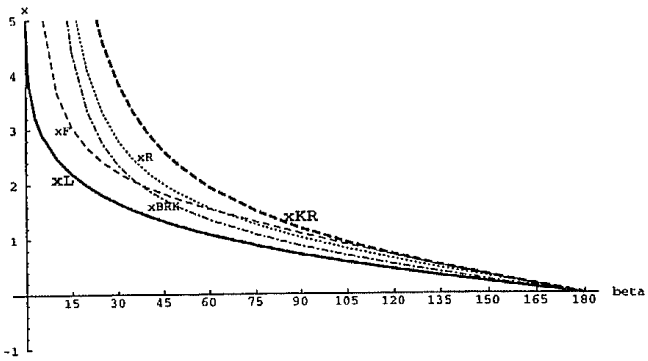

Fig. 14. Localization results of approaches in figure 12 that optimize a certain cornerness measure and yield only one extremum for an L-corner.

curves of approaches from figure 12 that optimize a certain cornerness measure and, in addition, yield only one extremum for an L-corner, and we have plotted them again in figure 14. The best result relative to x_L is obtained with the approaches of Förstner [13] and of Blom et al. [5], which are indicated by the positions x_F and x_{BRK}, respectively. For $\beta \lesssim 35°$ the curve of x_F is closest to x_L, whereas for $\beta \gtrsim 35°$ this is the case for x_{BRK}. It is interesting that the curve of x_{BRK} is close to the curve of x_{DN}. If the units of the x axis are identified with pixel positions, for $\beta > 20°$ (10°) the (absolute) deviation of x_F from x_L is smaller than 0.7 (1.3) pixels. For $\beta \gtrsim 65°$ the localization x_R using the approach in Rohr [24] is slightly better than x_F. The distance of the positions x_{KR} (result-

ing from the measure in Kitchen and Rosenfeld [16]) to x_L is always larger than for x_F, x_{BRK}, and x_R. The positive extremum x_{Bp} found with DET by Beaudet [1] is furthest from x_L, and for decreasing values of β it is asymptotic to the curve of x_{KR}. For $\beta \lesssim 65°$ (35°, 20°) the position x_{Bn} is closer to x_L than $x_{KR}(x_R, x_{BRK})$, and for $\beta \lesssim 7°$ the localization is better than for all other approaches. With the approach of Zuniga and Haralick [30] no corner points can be localized without incorporating edge points. We have also shown that the conditions of Nagel [20] for the gray-value surfaces investigated in the present paper cannot be used for determining corners.

If we consider the results with respect to localizing the point x_0, then for $\beta \lesssim 135°$ the positions x_{Bn} are the best (remember that we assumed $x_0 = 0$; see figures 1 and 12). In the whole range of $0° < \beta < 180°$ the absolute deviation from x_0 is always smaller than 0.9 pixels. For $\beta = 90°$ x_0 is located exactly.

It is also worth noting that for small angles β enormous deviations can occur. For $\beta = 1°$, for example, the deviation of x_{Bp} and x_{KR} with respect to x_L is larger than 100 pixels. For more realistic values, e.g., $\beta = 10°$, we have $x_{Bp} \approx x_{KR} \approx 11.5$ pixels (the deviation with respect to x_L is approximately 9 pixels); i.e., assuming the blur of the original image to be $\sigma_0 = 1$ and processing the image with a Gaussian filter of $\sigma_F = 1$ (2) leads to a displacement of the positions of $\Delta x = ((\sigma_0^2 + \sigma_F^2)^{1/2} - \sigma_0)x_{Bp} \approx 4.8$ (14.2) pixels. In these cases, approaches that track those points for different amounts of image smoothing may have problems (see, e.g., [9]).

Since real images are discretized, quantized, and corrupted by noise, in further investigations the influence of these effects on the performance of the different corner detectors should be analyzed.

Appendix

Partial derivatives of the model function $g(x, y)$ used in section 4 are as follows:

$$g_x = \tilde{g}_x,$$

$$g_y = 2y\tilde{g}_y;$$

$$g_{xx} = \tilde{g}_{xx},$$
$$g_{xy} = 2y\tilde{g}_{xy},$$
$$g_{yy} = 2(\tilde{g}_y + 2y^2\tilde{g}_{yy});$$

$$g_{xxx} = \tilde{g}_{xxx},$$
$$g_{xxy} = 2y\tilde{g}_{xxy},$$
$$g_{xyy} = 2(\tilde{g}_{xy} + 2y^2\tilde{g}_{xyy}),$$
$$g_{yyy} = 4y(3\tilde{g}_{yy} + 2y^2\tilde{g}_{yyy});$$

$$g_{xxxx} = \tilde{g}_{xxxx},$$
$$g_{xxxy} = 2y\tilde{g}_{xxxy},$$
$$g_{xxyy} = 2(\tilde{g}_{xxy} + 2y^2\tilde{g}_{xxyy}),$$
$$g_{xyyy} = 4y(3\tilde{g}_{xyy} + 2y^2\tilde{g}_{xyyy}),$$
$$g_{yyyy} = 4(3\tilde{g}_{yy} + 12y^2\tilde{g}_{yyy} + 4y^4\tilde{g}_{yyyy});$$

$$g_{xxyyy} = 4y(3\tilde{g}_{xxyy} + 2y^2\tilde{g}_{xxyyy}).$$

Acknowledgment

For discussions and helpful comments I thank J. Rieger, C. Schnörr, B. Neumann, G. Winkler, D. Bister, K. Daniilidis, C. Drewniok, D. Koller, H. Neumann, and G. Retz-Schmidt. I am grateful to J. Rieger for his suggestion to use the lemma of Whitney.

References

1. P.R. Beaudet, "Rotationally invariant image operators," in *Proc. International Joint Conference on Pattern Recognition*, Kyoto, Japan, 1978, pp. 579–583.
2. F. Bergholm, "Edge focusing," *IEEE Trans. Patt. Anal. Mach. Intell.*, vol. PAMI 9, pp. 726–741, 1987.
3. F. Bergholm and K. Rohr, "A comparison between two approaches applied for estimating diffuseness and height of step edges," Fraunhofer Institute for Information and Data Processing (IITB), Karlsruhe, Germany, House Rep. 10262, 1991; see also Department of Analysis and Computing Science, Royal Institute of Technology, Stockholm, Tech. Rep. TRITA-NA-P9105, CVAP 83, 1991.
4. V. Berzins, "Accuracy of Laplacian edge detectors," *Comput. Vis., Graph., Image Process.*, vol. 27, pp. 195–210, 1984.
5. J. Blom, B.M. ter Haar Romeny, and J.J. Koenderink, "Affine invariant corner detection," submitted for publication; see also J. Blom, "Topological and geometrical aspects of image structure," doctoral dissertation, University of Utrecht, The Netherlands, 1992.

6. I.N. Bronstein and K.A. Semendjajew, *Taschenbuch der Mathematik*, 19th ed., Verlag Harri Deutsch: Frankfurt, 1981.
7. K. Brunnström, T. Lindeberg, and J.-O. Eklundh, "Active detection and classification of junctions by foveation with a head-eye system guided by the scale-space primal sketch," in *Proc. 2nd European Conference on Computer Vision*, S. Margherita, Italy, 1992; Lecture Notes in Computer Science, vol. 588, G. Sandini, (ed.), Springer-Verlag: Berlin, pp. 701–709, 1992.
8. F. Canny, "A computational approach to edge detection," *IEEE Trans. Patt. Anal. Mach. Intell.*, vol. PAMI-8, pp. 679–698, 1986.
9. R. Deriche and G. Giraudon, "Accurate corner detection: an analytical study," in *Proc. 3rd International Conference on Computer Vision*, Osaka, Japan, 1990, pp. 66–70.
10. L. Dreschler, "Zur Reproduzierbarkeit von markanten Bildpunkten bei der Auswertung von Realwelt-Bildfolgen," in *Modelle und Strukturen*, DAGM Symposium, Hamburg, Germany, 1981, Informatik-Fachberichte 49, B. Radig, ed., Springer-Verlag: Berlin, 1981, pp. 76–82.
11. L. Dreschler and H.-H. Nagel, "Volumetric model and 3D-trajectory of a moving car derived from monocular TV-frame sequences of a street scene," in *Proc. International Joint Conference of Artificial Intelligence*, Vancouver, Canada, 1981, pp. 692–697; see also *Computer Graph. Image Process.* vol. 20, pp. 199–228, 1982.
12. W. Förstner, "On the geometric precision of digital correlation," *Int. Arch. Photogramm. Remote Sensing*, vol. 24, pp. 176–189, 1982.
13. W. Förstner, "A feature based correspondence algorithm for image matching," *Int. Arch. Photogramm. Remote Sensing*, vol. 26, pp. 150–166, 1986.
14. G. Giraudon and R. Deriche, "On corner and vertex detection," in *Proc. IEEE Conference on Computer Vision and Pattern Recognition*, Lahaina, Maui, Hawaii, 1991, pp. 650–655.
15. A. Guiducci, "Corner characterization by differential geometry techniques," *Patt. Recog. Let.*, vol. 8, pp. 311–318, 1988.
16. L. Kitchen and A. Rosenfeld, "Gray-level corner detection," *Patt. Recog. Lett.*, vol. 1, pp. 95–102, 1982.
17. A. Korn, "Toward a symbolic representation of intensity changes in images," *IEEE Trans. Patt. Anal. Mach. Intell.*, vol. PAMI-10, pp. 610–625, 1988.
18. J. Martinet, *Singularities of Smooth Functions and Maps*, London Mathematical Society Lecture Note Series 58, Cambridge U. Press: Cambridge, England, 1982.
19. E. De Micheli, B. Caprile, P. Ottonello, and V. Torre, "Localization and noise in edge detection," *IEEE Trans. Patt. Anal. Mach. Intell.*, vol. PAMI-11, pp. 1106–1117, 1989.
20. H.-H. Nagel, "Displacement vectors derived from second-order intensity variations in image sequences," *Comput. Vis., Graph., Image Process.*, vol. 21, pp. 85–117, 1983.
21. H.-H. Nagel, "Constraints for the estimation of displacement vector fields from image sequences," *Proc. International Joint Conference on Artificial Intelligence*, Karlsruhe, Germany, 1983, pp. 945–951.
22. J.A. Noble, "Finding corners," in *Proc. 3rd Alvey Vision Conference*, Cambridge, England, 1987, pp. 267–274.
23. J.H. Rieger, "Generic properties of edges and 'corners' on smooth greyvalue surfaces," *Biol. Cybernet.*, vol. 66, pp. 497–502, 1992.
24. K. Rohr, "Untersuchung von grauwertabhängigen Transformationen zur Ermittlung des optischen Flusses in Bildfolgen," Diplomarbeit, Institut für Nachrichtensysteme, Universität Karlsruhe, Germany, 1987.
25. K. Rohr, "Über die Modellierung und Identifikation charakteristischer Grauwertverläufe in Realweltbildern," in *12th DAGM – Symposium Mustererkennung*, Informatik-Fachberichte 254, R.E. Großkopf, ed., Springer-Verlag: Berlin, 1990, pp. 217–224.
26. K. Rohr, "Modelling and identification of characteristic intensity variations," *Image Vis. Comput.*, vol. 10, pp. 66–76, 1992.
27. K. Rohr, "Recognizing corners by fitting parametric models," *Int. J. Comput. Vis.*, vol. 9, pp. 213–230, 1992.
28. K. Rohr and C. Schnörr, "An efficient approach to the identification of characteristic intensity variations," *Image Vis. Comput.*, vol. 11, pp. 273–277, 1993.
29. M.A. Shah and R. Jain, "Detecting time-varying corners," *Proc. 7th International Conference on Pattern Recognition*, Montreal, Canada, 1984, pp. 2–5.
30. O.A. Zuniga and R.M. Haralick, "Corner detection using the facet model," in *Proc. IEEE Conference on Computer Vision and Pattern Recognition*, Washington, D.C. 1983, pp. 30–37.

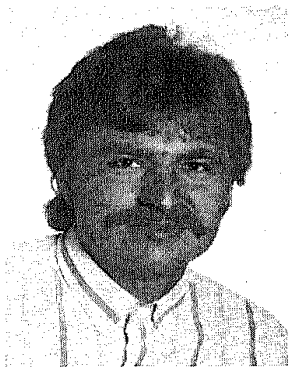

Karl Rohr received his Diploma degree in electrical engineering from the University of Karlsruhe, Germany, in 1987. From 1988 to 1991 he was with the Department of Computer Science, University of Karlsruhe, and currently he is with the Department of Computer Science, University of Hamburg, Germany.

In 1990 he was awarded a DAGM prize for his paper on model-based recognition of gray-value corners. His research interests include computer vision, with particular emphasis on low-level vision, and computer graphics.